Biophysical Journal
Article

Biophysical Society

ECM Cross-Linking Regulates Invadopodia Dynamics

Kamyar Esmaeili Pourfarhangi,[1] Aviv Bergman,[2,3] and Bojana Gligorijevic[1,4,*]
[1]Bioengineering Department, College of Engineering, Temple University, Philadelphia, Pennsylvania; [2]Systems & Computational Biology Department, Albert Einstein College of Medicine, New York, New York; [3]Santa Fe Institute, Santa Fe, New Mexico; and [4]Cancer Biology Program, Fox Chase Cancer Center, Philadelphia, Pennsylvania

ABSTRACT Invadopodia are membrane protrusions dynamically assembled by invasive cancer cells in contact with the extracellular matrix (ECM). Invadopodia are enriched by the structural proteins actin and cortactin as well as metalloproteases such as MT1-MMP, whose function is to degrade the surrounding ECM. During metastasis, invadopodia are necessary for cancer cell intravasation and extravasation. Although signaling pathways involved in the assembly and function of invadopodia are well studied, few studies address invadopodia dynamics and how the cell-ECM interactions contribute to cell invasion. Using iterative analysis based on time-lapse microscopy and mathematical modeling of invasive cancer cells, we found that cells oscillate between invadopodia presence and cell stasis—termed the "invadopodia state"—and invadopodia absence during cell translocation—termed the "migration state." Our data suggest that β1-integrin-ECM binding and ECM cross-linking control the duration of each of the two states. By changing the concentration of cross-linkers in two-dimensional and three-dimensional cultures, we generate an ECM in which 0–0.92 of total lysine residues are cross-linked. Using an ECM with a range of cross-linking degrees, we demonstrate that the dynamics of invadopodia-related functions have a biphasic relationship to ECM cross-linking. At intermediate levels of ECM cross-linking (0.39), cells exhibit rapid invadopodia protrusion-retraction cycles and rapid calcium spikes, which lead to more frequent MT1-MMP delivery, causing maximal invadopodia-mediated ECM degradation. In contrast, both extremely high or low levels of cross-linking lead to slower invadopodia-related dynamics and lower ECM degradation. Additionally, β1-integrin inhibition modifies the dynamics of invadopodia-related functions as well as the length of time cells spend in either of the states. Collectively, these data suggest that β1-integrin-ECM binding nonlinearly translates small physical differences in the extracellular environment to differences in the dynamics of cancer cell behaviors. Understanding the conditions under which invadopodia can be reduced by subtle environment-targeting treatments may lead to combination therapies for preventing metastatic spread.

INTRODUCTION

Invadopodia (1) are dynamic membrane protrusions involved in the invasive motility of cancer cells. Their function is to degrade the surrounding extracellular matrix (ECM). In tumors in vivo, they are necessary for cancer cell intravasation into (2) and extravasation (3) out of the blood vessels. In vitro, invasive cancer cells assemble invadopodia when grown on various ECM components and in the presence of growth factors. Invadopodia have the appearance of puncta rich in actin, actin-regulatory proteins (e.g., cortactin), tyrosine kinases, and proteases (e.g., MT1-MMP). Although a large number of invadopodia components are found in other motility-related structures such as focal adhesions and lamellipodia, the unique feature of invadopodia is the high ECM-degrading activity.

Assembly and maturation of an individual invadopodium has been well studied (4,5) using two-dimensional (2D) in vitro assays. Invadopodium precursors consisting of cortactin, cofilin, and N-WASP are first assembled (6). The structure is then stabilized via focal adhesion proteins such as β1-integrin by binding the structure tip to the ECM (7,8). During invadopodia maturation, cortactin phosphorylation leads to continuous actin polymerization and MT1-MMP recruitment to the tips of the invadopodia via late endosomes (9). Transmembrane MT1-MMP assures focalized ECM degradation of the surrounding ECM, and the invadopodia become mature and functional (at ~50 min) (6). During ECM-degrading activity, mature invadopodia exhibit calcium spikes dependent on store-operated calcium entry, which are necessary for MT1-MMP recycling to the plasma membrane (10). Mature

Submitted October 13, 2017, and accepted for publication January 22, 2018.

*Correspondence: bojana.gligorijevic@temple.edu

Editor: Vivek Shenoy.
https://doi.org/10.1016/j.bpj.2018.01.027

invadopodia also exert physical forces on the ECM by means of protrusion-retraction cycles, during which actin filaments polymerize (protrusion) and depolymerize (retraction) repeatedly (11). Physical and proteolytic ECM remodeling by invadopodia are coordinated via cortactin (de)phosphorylation and positive feedback from MT1-MMP (12,13).

The assembly of invadopodia and the level of ECM degradation were shown to be linked to ECM properties such as rigidity, density, and cross-linking (14–16). This points to the essential role in adhesion-based signaling in the invadopodia progression. A recent study of β1-integrin's role in invadopodia strengthened this link, demonstrating that β1-integrin is localized to invadopodia and directly links the structure to the ECM (7). Although elimination of β1-integrin does not inhibit invadopodia precursor assembly, it disables invadopodia maturation and the ECM-degrading function.

Recent studies of invadopodia in three dimensions (13,17,18) and in vivo (2,19) demonstrated that invadopodia are present at the front of the cells migrating in an MMP-dependent manner. Depending on the ECM parameters, including density, fiber size, stiffness, and/or cross-linking, such migration can result in a broad range of speeds (6–30 μm/h for breast carcinoma) (13,20,21). In vivo, the presence of invadopodia was also shown to be highly dependent on ECM cross-linking (2). Although the studies of three-dimensional (3D) and in vivo invadopodia established the link between invadopodia and cell movement, it is not known if cells that assemble invadopodia can translocate the cell body simultaneously or if they move and assemble invadopodia in a sequential manner.

We used iterative cycles of time-lapse microscopy and mathematical modeling to address the role of invadopodia dynamics and ECM cross-linking in invasive cell motility. We found that the dynamics of invadopodia assembly and function have a nonmonotonic (biphasic) relationship with increases in ECM cross-linking. Furthermore, we show that the presence of invadopodia and the migration of cells are negatively correlated, with the level of active β1-integrin controlling the duration of each of the two states. We demonstrate that partial blocking of β1-integrin increases the duration of migration and shortens the period of active ECM degradation by inhibiting invadopodia activity. Taken together, our results suggest that invadopodia-driven, MMP-dependent motility consists of oscillations between 1) sessile invadopodia assembly leading to ECM degradation and 2) migration. Modulation of β1-integrin activity or ECM cross-linking can be used to reduce or eliminate invadopodia, which are necessary for intravasation and metastasis (2).

METHODS

Cell culture

The mouse breast carcinoma line Cerulean-cortactin-MTLn3 was a gift from Dr. Ved Sharma from Albert Einstein College of Medicine (22). The cells were cultured in α-minimal essential medium (Gibco, Thermo Fisher Scientific, Waltham, MA), supplemented with 5% fetal bovine serum (FBS) (Gemini Bio Products, West Sacramento, CA), penicillin-streptomycin mixture (Gibco, Thermo Fisher Scientific), and 0.5 mg/mL G418 (Sigma-Aldrich, St. Louis, MO). Cerulean-LifeAct-MDA-MB-231 and Cerulean-LifeAct-H2B-GFP cell lines were generated using the mCerulean3-LifeAct-7 plasmid, selected with 0.5 mg/mL G418 over a 4-week period and purified by fluorescence-activated cell sorting. mCerulean3-LifeAct-7 was a gift from Michael Davidson (plasmid #54721; Addgene, Cambridge, MA). Cells from the human cell lines MDA-MB-231 and Hs-578T (American Type Culture Collection, Manassas, VA) were cultured in Dulbecco's modified eagle medium (Gibco, Thermo Fisher Scientific), supplemented with 10% FBS and 1% penicillin-streptomycin. For Hs-578T cells, 1 mM pyruvate (Gibco, Thermo Fisher Scientific) and 0.01 mg/mL bovine insulin (Sigma-Aldrich) were added to the culture media.

Cumulative degradation of gelatin layer

MTLn3, MDA-MB-231, and Hs578T cells were cultured on the gelatin-coated plates (~500 nm thick) described previously (22). Briefly, acid-washed 35 mm MatTek (MatTek Corporation, Ashland, MA) dishes were treated with 50 μg/mL poly-L-lysine (Gibco, Thermo Fisher Scientific) for 20 min and then incubated with Alexa 488 dye-labeled gelatin (Sigma-Aldrich) for 10 min. Plates were then washed with phosphate-buffered saline (PBS) (Gibco, Thermo Fisher Scientific) and cross-linked by glutaraldehyde (GTA) (Sigma-Aldrich) on ice for 15 min (from 0.0 to 5.0% v/v GTA in water), extensively rinsed with PBS, quenched with 5 mg/mL sodium borohydride (Sigma-Aldrich), and sterilized with 70% ethanol (Decon Laboratories, King of Prussia, PA).

60,000 cells per dish were plated for 18 h on 35 mm MatTek dishes. Cells were fixed with 4% vol paraformaldehyde (Electron Microscopy Sciences, Hatfield, PA) for 15 min and permeabilized with 0.1% Triton X-100 (Sigma-Aldrich) for 10 min. Fixed cells were then blocked in 1% bovine serum albumin (fraction V; Sigma-Aldrich) and 1% FBS for 2 h, incubated at 1:100 with anti-cortactin antibody (ab-33333; Abcam, Cambridge, UK) for 2 h, and incubated for 2 h with Alexa-Fluor-633 (1:250) and Alexa-Fluor-546-Phalloidin (1:250) (Abcam).

Imaging of the invadopodia precursors and cumulative degradation at 18 h were performed using an Olympus FluoView 1200 confocal microscope (Olympus, Tokyo, Japan) with sequential imaging of 6 $\times$ 1 μm z-sections per stack.

Invadopodia degradation was assessed by quantifying the area of degradation per cell and the number of invadopodia precursors (colocalization of actin and cortactin) per cell at each condition in Fiji (23). For area of degradation, thresholding and particle size analysis were performed using Fiji. Experiments were done in triplicates by imaging >10 fields of view and >100 cells in each sample.

3D FITC-DQ collagen I assay

100,000 MTLn3 cells were suspended in 100 μL of collagen mixture containing the following: 1.5 mg/mL collagen (Corning, Tewksbury, MA), 50 mM Tris-HCl, 2.5 mM CaCl2, 1 mM dithiothreitol (Sigma-Aldrich), 0.15 mg/mL fluorescein isothiocyanate-dequenched (FITC-DQ) collagen I (Molecular Probes, Thermo Fisher Scientific), and transglutaminase II (TGII) (R&D Systems, Minneapolis, MN) at 1:50,000-1:800,000 dilution. Similarly to GTA, TGII cross-links free amine groups of glutamine and lysine residues of collagen I (24). The mixture was pipetted in a 35 mm MatTek dish and incubated at 37°C for 30 min, forming a 650-μm-thick 3D cell culture. 2 mL of media (α-minimal essential medium and 5% FBS) was pipetted into the plate. At 0 and 42 h, 10 image stacks (20 $\times$ 5 μm) were collected. An Olympus FluoView FV1200 confocal microscope (Olympus) was used, with 488 nm laser excitation.

3D collagen degradation was assessed by measuring the area positive for DQ collagen at each condition. Briefly, images captured at 42 h were thresholded, and particle analysis was used in Fiji to quantify the area positive for FITC-DQ collagen fluorescence. Measured values were subtracted from negative controls treated with GM6001 MMP inhibitor. All measurements were done in 10 fields of view per sample, with three biological repeats per condition.

3D collagen pore size measurement

3D cultures embedded in FITC-DQ collagen I and cross-linked to different degrees were imaged by reflection confocal microscopy. Images were thresholded with the "yen" algorithm in Fiji, filtered using a LoG 3D plug-in, and thresholded again with "yen" to get the binary image of the pores. Finally, particle analysis was used to measure the size of the pores.

Cross-linking degree measurements

Measurement of cross-linking degree followed previously published techniques (24,25). Briefly, 0.2% weight per volume gelatin samples were mixed with 0.0–5.0% v/v GTA and incubated on ice for 10 min. Cross-linking was quenched with 5 mg sodium borohydride for 15 min. For collagen, a mixture of 1.5 mg/mL collagen I in PBS, 50 mM Tris-HCl, 2.5 mM CaCl2, and 1 mM dithiothreitol was cross-linked with 1:0.5K–1:800K TGII:collagen at 37°C for 30 min.

Non-cross-linked amino groups were neutralized by incubation with 4% $NaHCO_3$ and 0.5% trinitrobenzenesulfonic acid (Sigma-Aldrich) for 2 h at 37°C in the dark. Finally, samples were incubated at 37°C for 1 h with 6 M HCL (Sigma-Aldrich). The absorbance was measured at 345 nm using an Infinite M200 PRO plate reader (Tecan, Männedorf, Switzerland).

Live cell imaging

Live cell imaging was performed for invadopodia lifetime, cortactin oscillations, and calcium spike analysis. In brief, Cerulean-cortactin-MTLn3 cells were cultured on MakTek dishes coated with Alexa 488 or 546 gelatin and incubated in culture conditions for 16 h. For lifetime analysis and cortactin oscillations, the media were changed to L-15 with 5% FBS, 1:100 Oxyfluor (Oxyrase, Mansfield, OH), and 10 mM sodium lactate (Sigma-Aldrich) as reactive oxygen scavengers. Dishes were placed in a 37°C live-cell imaging chamber, and time-lapse imaging was performed on a widefield Olympus IX81 microscope (Olympus) equipped with an LED lamp, Hamamatsu Orca 16-bit charge-coupled device (Hamamatsu, Hamamatsu, Japan), automated z-drift compensation IX3-ZDC (Olympus), automated Prior stage (Prior Scientific, Rockland, MA), and environmental chamber. An Olympus 60X 1.4 NA Oil M Plan Apochromat objective was used.

Measurement of invadopodia stability

Images were captured every 10 min for >16 h (1.67 mHz). Invadopodia lifetimes were measured in Fiji and defined as the time between appearance and disappearance of cortactin punctae. Punctae present at the first or last frames were not taken into account. The invadopodia stability ratio was defined as the ratio of the number of mature invadopodia (those with lifetimes of >50 min (6)) to the total number of invadopodia.

Cortactin oscillations in invadopodia core

Images were collected every 30 s (33.3 mHz) for 4 h. Oscillations of cortactin fluorescence were measured only in mature invadopodia (present >50 min). For inhibiting F-actin polymerization, 4 μM cytochalasin D (Sigma-Aldrich) was added to the media before imaging. In Fiji, we filtered individual invadopodia precursors with a LoG 3D (26) plug-in and tracked the centers of the invadopodia in all frames by SpotTracker (26). A custom-written Fiji plug-in was used to measure the average signal inside the invadopodium as well as 4–8 circular areas inside the cytoplasm at each particular frame. In MATLAB (The MathWorks, Natick, MA), fast Fourier transform was applied to the time-resolved cortactin signal in the invadopodia and the surrounding cytoplasmic regions. High frequencies from the cytoplasm were removed, and the filtered invadopodia signal was returned to the time domain by inverse fast Fourier transform. Finally, the MATLAB autocorrelation function was used to measure oscillation frequencies in the invadopodia.

Calcium spikes

After cells were plated for 16 h, cells were incubated for 15 min at room temperature in L-15, 2.5 mM probenecid (Life Technologies, Frederick, MD), 2.5 μM Fluo4-AM (Life Technologies), and 0.02% Pluronic (Life Technologies) (10). Cells were then washed twice with PBS and incubated in L-15 with 5% FBS for 30 min at 37°C. Time-lapse imaging was performed at 5 s intervals (200 mHz) for 1 h. Cytoplasmic calcium spikes were measured by monitoring intracellular Fluo-4-AM signals over time (10). In Fiji, entire cells were used as regions of interest; background subtraction was done by subtracting the fluorescent signal measured in inactive regions. Measurements of inactive cells (~70% of total, <10 spikes per hour) were not taken into account (10,27). In MATLAB, power spectrum was applied to the time-resolved signal in the cytoplasm. Dominant frequencies at different conditions were further compared.

Measurement of the MT1-MMP delivery event frequency

To visualize the MT1-MMP delivery event to the plasma membrane, Hs-578T cells were transiently transfected with MT1-MMPpHluorin 24 h before imaging. Transfection was performed via an electroporation technique, in which a 2 μg plasmid vector was mixed with 1×10^6 cells and 50 μL nucleofection solution R (Lonza, Basel, Switzerland). Nucleofection was then performed on the mixture using program X-001 of a nucleofector device (Lonza). Transfected cells were then plated in a glass-bottom plate, and 24 h after plating, 30 min time-lapse movies were captured from the cells using a 488 nm laser. A delivery event was defined as the moment that MT1-MMP flashes appeared, and the rate of delivery was measured as one over the average of the interval between successive flashes.

β1-integrin-blocking assay

The blocking of β1-integrin activity was done by applying a 4B4 β1-integrin-blocking antibody (Beckman Coulter, Brea, CA) at doses of 0, 0.4, 0.6, and 2 μg/mL to the cultures 2 h after plating the cells. MDA-MB-231 cells were plated at a density of 60,000/x cm^2 on Alexa 488 gelatin-coated dishes, and time-lapse movies were recorded. Displacement of the cells over time was measured using the Fiji plug-in TrackMate (28). For area of degradation, thresholding and particle size analysis were performed using Fiji. Experiments were done in triplicates by imaging >10 fields of view and >100 cells in each sample.

Statistical analysis

A one-way analysis of variance with Tukey's multiple-comparison posttests was performed to compare the 2D and 3D invadopodia degradation data. A two-tailed Student's *t*-test was performed for statistical analysis as indicated, and the statistical significance was defined as $^*p < 0.05$, $^{**}p < 0.01$, and $^{***}p < 0.001$. Data are shown as mean ± SE.

RESULTS

Breast cancer cells switch from migration to invadopodia-mediated ECM degradation

To determine whether cell migration occurs simultaneously or sequentially with invadopodia assembly, we acquired time-lapse recordings of >100 cells in each of the two breast carcinoma cell lines known to spontaneously assemble invadopodia (MTLn3 and MDA-MB-231). Cells were engineered to stably express fluorescent invadopodia markers (Cerulean-cortactin or Ceruelan-LifeAct) and cultured on fluorescent Alexa 488 gelatin (Movies S1 and S2). Recordings were scored by tracking the centroid path over time (Fig. 1, *A–C*, *path*) as well as quantifying the number of invadopodia (Fig. 1 *C*, *cyan punctae*).

In the beginning of Movie S1, the tracked cell migrates relatively fast (>0.3 μm/min or >18 μm/h) (Fig. 1 *D*, *red trace*). Although the cell assembles several short-living (<10 min lifetime) invadopodia precursors characterized by cortactin-enriched punctae, none of them result in any detectable ECM degradation. Starting at 380 min, the speed of the cell decreases (<0.2 μm/min), and the cell assembles mature invadopodia characterized by cortactin-enriched punctae with >50 min lifetimes colocalized with ECM degradation (Movie S1, *red circles*, and Fig. 1 *D*, *blue trace*). Similar observations were next confirmed in the MDA-MB-231 cells (Movie S2), in which several cycles of switching between migration and mature invadopodia were observed (Fig. 1 *E*).

Based on these observations, we defined two oscillating cell states: migration state, in which cells exhibit speeds of >0.3 μm/min and no ECM degradation, and invadopodia state, in which cells exhibit punctae rich in cortactin (or actin) colocalized with ECM degradation and migrate at speeds of <0.2 μm/min.

Our previous work in vivo suggested that the balance between migration and invadopodia is determined by ECM cross-linking (2). Moreover, ECM cross-linking has been

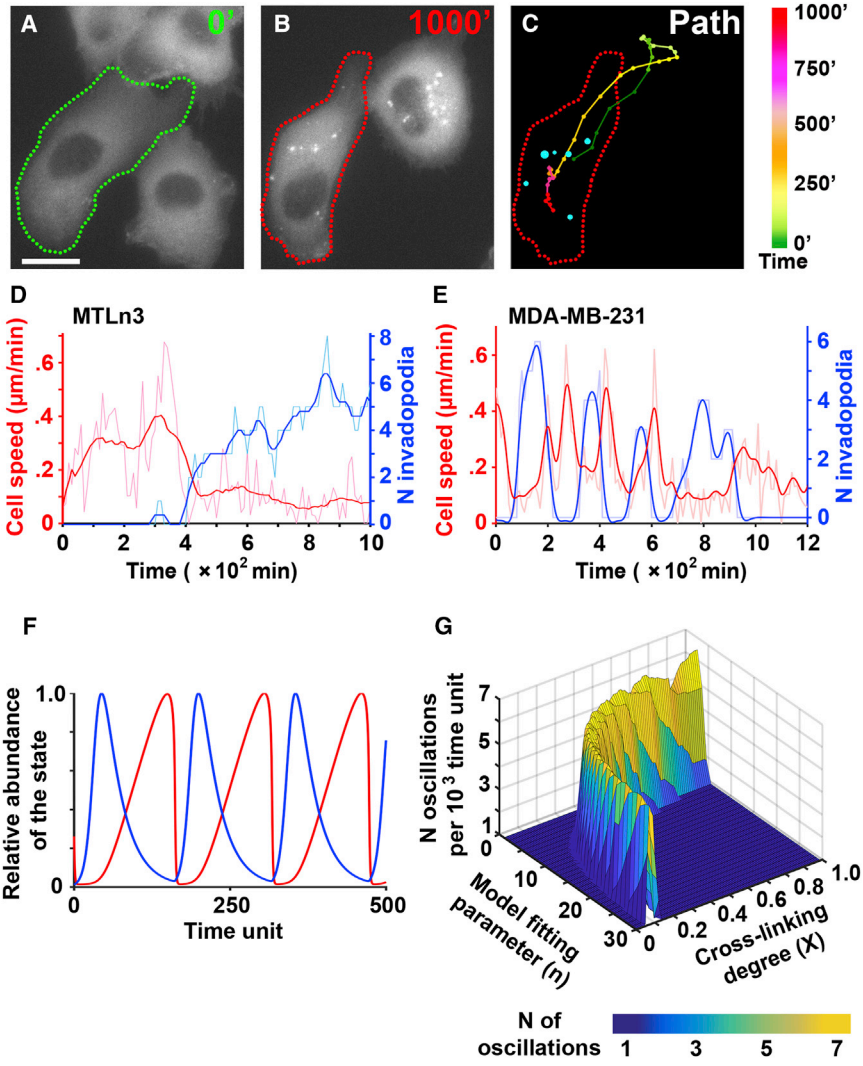

FIGURE 1 Oscillations between migration and invadopodia states in cancer cells and the role of ECM cross-linking. (*A*) The micrograph shows the Cerulean-cortactin-MTLn3 cell at time 0 of Movie S1. The cell border is highlighted with the green dotted line. Scale bars, 10 μm. (*B*) The same cell at 1000 min is highlighted in red. (*C*) A summary of (*A*) and (*B*) is shown, with color-coded path 0–1000 min and cyan punctae representing invadopodia at 1000 min. A color code legend is shown on the right. (*D* and *E*) Shown are quantifications of Movie S1 (Cerulean-cortactin-MTLn3) and Movie S2 (Cerulean-LifeAct-MDA-MB-231), respectively. Cell speed in μm/min (*red lines*) and number of invadopodia (*blue lines*) were recorded over time in representative cells. Raw data (*shaded lines*) and smoothened data (*bright lines*) are shown. (*F*) Shown is a simulation of cancer cell oscillations between invadopodia (*blue*, relative abundance I/I_{max} versus time) and migration (*red*, relative abundance M/M_{max} versus time). (*G*) Based on the results of the model, the number of invadopodia-migration oscillations shows a biphasic trend to linear changes in ECM cross-linking and the model-fitting parameter "n." To see this figure in color, go online.

demonstrated to enhance integrin signaling (29) and increase levels of ECM degradation by invadopodia (15). Hence, we hypothesized that the frequency of switching between the invadopodia state and migration state will be controlled by ECM cross-linking and integrin-driven ECM-cell interactions (20,21,29–32). To develop a generalizable prediction, we developed a phenomenological, nondimensional mathematical model (see Supporting Material) based on the observed state oscillations and prior studies on ECM-cell interactions in 2D, 3D, and in vivo environments.

The dynamic variables used in the model were the concentration of ECM interacting with the cell (represented by C_{ECM}), abundance of the invadopodia state (represented by I), and abundance of the migration state (represented by M). Cell-ECM interactions were assumed to be constant for specific ECM conditions and were addressed by the adhesion constant Ka. To address the dynamic properties of the migration and degradation oscillations, we varied the degree of ECM cross-linking (expressed as X, the ratio of cross-linked lysine residues to the total number of lysine residues). We additionally introduced a model-fitting parameter (n), which was used to fit the model to different ECM dimensionalities. Parameter "n" was further experimentally determined to be 6 in 2D assays and 7 in 3D conditions (Fig. S1).

Fig. 1 *F* shows one run of the model simulation for a cell oscillating between invadopodia (*blue line*) and migration (*red line*). The dynamics of the transition between invadopodia and migration states observed at a single-cell level (Fig. 1, *D* and *E*) are recapitulated and extended in the repeated cycles of migration and invadopodia that the model demonstrates. Fig. 1 *G* summarizes the model simulations for varying X, n, and oscillation frequencies. The model suggests that an increase in ECM cross-linking will enable a biphasic change in the frequency of migration and invadopodia switches in cells. Such a prediction implies that at an intermediate cross-linking X, the number of switches from migration to degradation and vice versa will reach a maximum (Fig. 1 *G*, *yellow regions*), which will in turn result in the maximal number of degraded punctae.

Invadopodium maturation and ECM degradation biphasically conform to ECM cross-linking in 2D and 3D

To test if the prediction of our model was supported in experimental invadopodia assays, we measured invadopodia assembly and function in the ECM with increasing cross-linking degrees. Breast carcinoma MTLn3 cells were plated on a thin fluorescent gelatin layer cross-linked from 0 to 0.92 cross-linking degree (Fig. S2 *A*) using the chemical cross-linker GTA. At 18 h after plating, the number of invadopodia precursors, mature invadopodia, and ECM degradation were measured (Fig. 2, *A–D*). The number of invadopodia precursors reached a plateau at 0.39 cross-linking degree (Fig. 2 *B*), whereas the number of mature invadopodia showed a strong biphasic trend with an increase in cross-linking (Fig. 2, *C* and *D*). The peak of the biphasic trend was at the intermediate cross-linking level (0.39) for both the total number of spots degraded over 18 h (Fig. 2 *C*) and for mature invadopodia present at the time of cell fixation (Fig. 2 *D*). Moreover, the portion of invadopodia precursors that mature and degrade ECM, reported as the invadopodia stability ratio, was at its maximum at the cross-linking degree of 0.39 (Fig. 2 *E*). The trend in increase of total area of degradation further confirms that the increase in the cross-linking degree has a biphasic relationship with invadopodia maturation and degradation. Our results were also confirmed using two additional human breast carcinoma cell lines: MDA-MB-231 and Hs-578T (Fig. 2 *F*). All three cell lines presented biphasic distributions of invadopodia-based degradation with increased cross-linking, with the peak at the intermediate cross-linking ($X = 0.39$). In conclusion, as predicted in our model, the experimental data show a biphasic trend in invadopodia degradation with an increased cross-linking ratio.

The results of the 2D invadopodia assay were then validated in a 3D invadopodia assay using FITC-DQ-collagen that was cross-linked using TGII from a 0 to 0.87 cross-linking degree (Fig. S2 *B*) (2,13,24,33). Colocalization of the FITC-DQ collagen I signal with cortactin, actin, and MT1-MMP confirmed that the 3D collagen degradation was due to invadopodia activity (Fig. 3 *A*). Interestingly, invadopodia-mediated degradation also followed a biphasic trend in a 3D environment, with maximal degradation present at an intermediate level of cross-linking (0.36) (Fig. 3 *B*).

Furthermore, measurements of collagen gel pore size and storage modulus revealed monotonic variation of these variables by increasing ECM cross-linking (Fig. S2, *C* and *D*). Biphasic variations of invadopodia-mediated ECM degradation as a response to monotonic changes of ECM cross-linking, pore size, and storage modulus pretermits passive regulation of invadopodia activity by ECM stiffening and suggests that invadopodia are actively responding to these changes at the molecular level.

Collectively, our model and experimental end-point measurements showed that the intermediate cross-linking degree results in the increase of the total number of invadopodia maturing and degrading the ECM over time. We hypothesized that this can be a result of faster dynamics of invadopodia activities, such as faster protrusive cycles and/or more frequent delivery of MT1-MMP.

Frequency of invadopodium protrusion-retraction cycles changes biphasically with an increase in ECM cross-linking

To assess the effect of ECM cross-linking on invadopodia protrusion-retraction cycles, the fluorescence intensity of

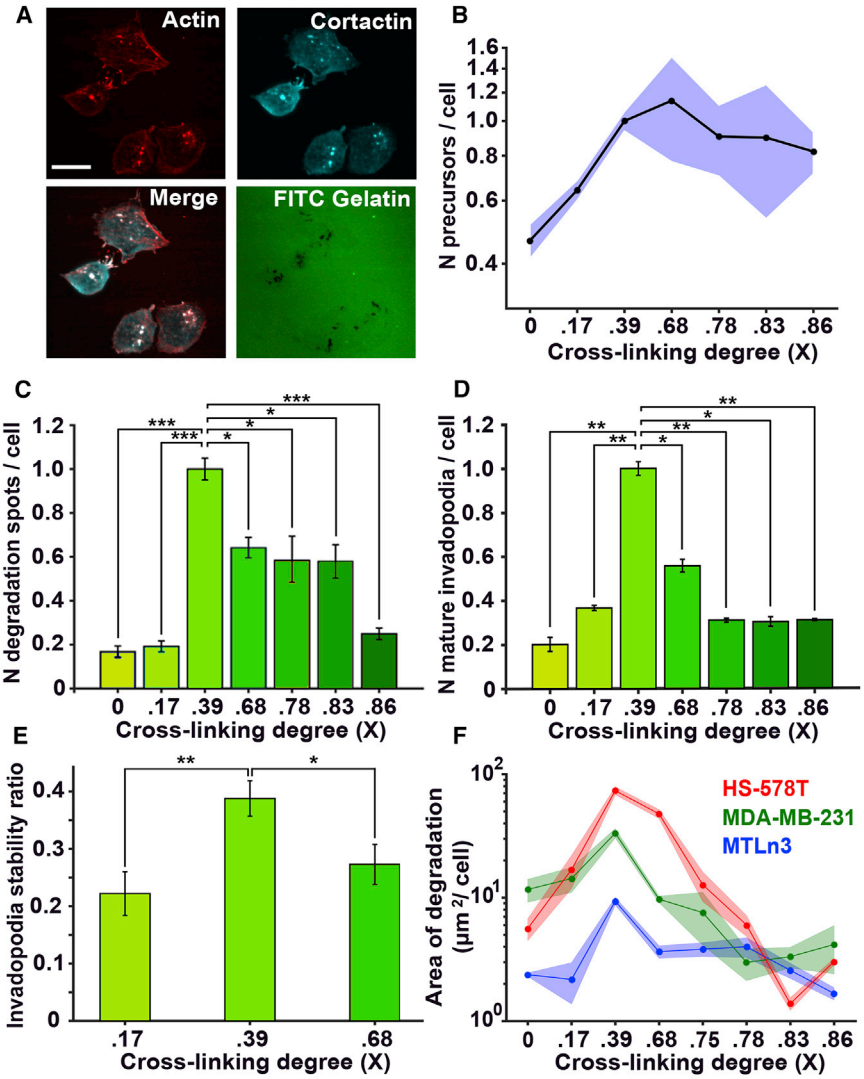

FIGURE 2 ECM cross-linking biphasically regulates invadopodia maturation and degradation. (*A*) Representative fluorescence micrographs show colocalization of actin (*red*) and cortactin (*cyan*) in invadopodia of MTLn3 cells. The lower-right panel shows degradation of gelatin at 18 h. Scale bars, 10 μm. (*B–D*) Shown are the relative number of invadopodia precursors (*B*), number of degradation spots (*C*), and number of mature invadopodia (*D*) at different cross-linker (GTA) concentrations in MTLn3 cells. In (*B*)–(*D*), the bars represent >300 cells in three separate experiments per condition; data are normalized to 0.05% GTA. (*E*) Shown is the invadopodia stability ratio at three concentrations of cross-linker; the bars represent >200 invadopodia in three separate experiments per condition; mean ± SE are shown. (*F*) Shown is the area of degradation measured at 18 h in three breast carcinoma cell lines: MTLn3 (*blue*), MDA-MB-231 (*green*), and Hs578 (*red*). Experiments are performed in triplicate, and circles represent the average degradation area per cell in >10 fields of view at each repeat. Lines represent mean values, and shaded areas represent 95% confidence intervals. In (*B*) and (*F*), vertical axes are in logarithmic scale. All *p*-values report comparison to a 0.39 cross-linking ratio condition. $*p < 0.05$, $**p < 0.01$, $***p < 0.001$. To see this figure in color, go online.

cortactin punctae (Movie S3) was monitored in MTLn3 cells at various gelatin cross-linking degrees (Fig. 4). Cortactin signal oscillations at invadopodia, reflecting the cycles of protrusion-retraction, were filtered (Fig. 4 *B*) and analyzed by autocorrelation (Fig. 4 *C*). The autocorrelation algorithm correlates the signal of the cortactin oscillations with delayed copies of itself to find the periodicity of a repeating pattern within the signal. Results show average frequencies of protrusion-retraction cycles of ~2.5 mHz at low or high (0.18 or 0.69) cross-linking degrees and a significantly higher frequency of 3.08 mHz at intermediate cross-linking (Fig. 4 *D*). This reflects significantly faster protrusion-retraction cycles and suggests that the dynamics of invadopodia protrusive cycles are in direct relationship to ECM cross-linking (Fig. 4 *D*). Furthermore, inhibiting F-actin polymerization by 4 μM cytochalasin D resulted in total abrogation of cortactin oscillations (Movie S4; Fig. 4, *E* and *F*), confirming that measured oscillations in cortactin signals reflect cycles of invadopodia protrusions and retractions. Combined with the results shown in Figs. 2 and 3, these data indicate that increased degradation at intermediate ECM cross-linking may be the consequence of faster protrusive cycles.

Next, we tested if the increase in ECM cross-linking affects proteolytic degradation of ECM by increased dynamics of calcium spikes and consequent MT1-MMP recycling to the plasma membrane (10).

Calcium spiking frequency biphasically changes with an increase in ECM cross-linking

Calcium spikes dependent on store-operated calcium entry were recently shown to be essential both for precursor assembly via Src activation and MT1-MMP recycling to the plasma membrane during ECM degradation (10). As calcium channels are commonly mechanosensitive (34–36) and calcium spiking can be influenced by ECM (37), we hypothesized that the frequency of calcium spikes will reach a

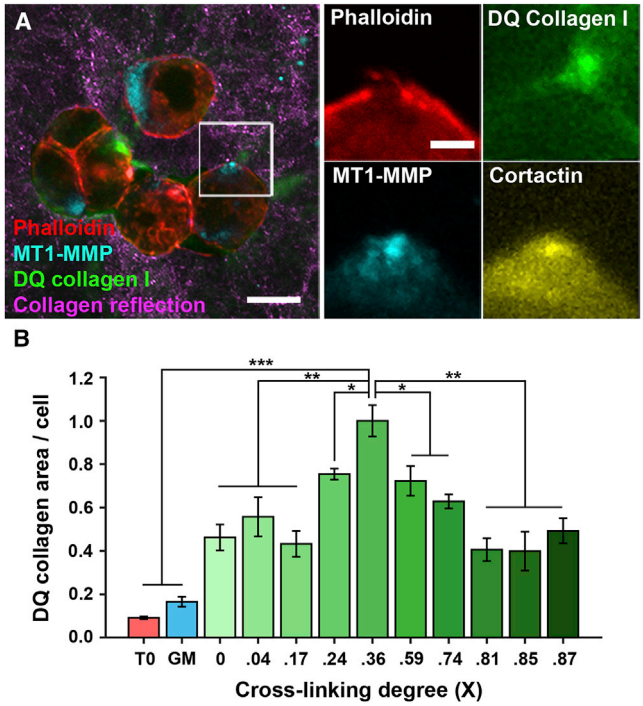

FIGURE 3 Collagen I cross-linking regulates ECM remodeling and degradation in three dimensions. (*A*) Representative fluorescence images depict MTLn3 cells in a 3D collagen I matrix. After 42 h, cells are fixed and immunostained for actin (*red*), cortactin (*yellow*), and MT1-MMP (*cyan*). Collagen fibers were detected with reflected confocal microscopy (*magenta*), and collagen degradation was measured using FITC-DQ collagen I (*green*). (*B*) Shown are FITC-DQ collagen-positive areas in 3D cultures. Green bars present FITC-DQ collagen-positive areas measured at 42 h postembedding into collagen with different cross-linking degrees. The red bar (T0) represents 0 h; the blue bar (GM) represents culture after 42 h treatment with GM6001, both at a cross-linking degree of 0.36. Experiments are performed in triplicate, and bars represent the average area per cell in >10 fields of view at each repeat. All *p*-values report comparison to the condition with 0.36 cross-linking ratio. $*p < 0.05$, $**p < 0.01$, $***p < 0.001$. To see this figure in color, go online.

peak value at a cross-linking degree of 0.39, in coordination with protrusion-retraction dynamics. To test this, we monitored calcium spikes in MTLn3 cells with invadopodia, recording Fluo-4-AM signals at different cross-linking degrees (Movie S5; Fig. 5, *A* and *B*). Dominant frequencies of calcium spikes were determined by power spectrum analysis (Fig. 5 *C*). Consistent with our model, calcium spikes are fastest at the intermediate cross-linking level (Fig. 5 *D*). Next, we tested if the fastest calcium spikes resulted in a more frequent delivery of MT1-MMP vesicles to the invadopodia plasma membrane.

MT1-MMP-containing vesicle delivery to the plasma membrane is biphasically regulated by ECM cross-linking

MT1-MMP is recycled by acidic late endosomes to the tip of mature invadopodia, where it is exocytosed to the neutral environment. We tested the MT1-MMP delivery rate using pH-sensitive MT1-MMPpHluorin. This fluorescent protein marks the exocytic events of MT1-MMP, which appear as GFP-positive blinking spots colocalized with the invadopodia (38). The exocytosis of MT1-MMPpHluorin vesicles was monitored at different cross-linking ratios (Movie S6; Fig. 5, *E* and *F*) to calculate the average vesicle delivery rate for each condition. At a cross-linking ratio of 0.39, MT1-MMP-vesicles were delivered more frequently compared to other cross-linking ratios (Fig. 5, *F* and *G*). Interestingly, frequencies of calcium spikes and MT1-MMP vesicle delivery operated in a similar range, suggesting a coordination between cycles of calcium spikes and vesicle delivery (37).

Collectively, our data suggest that frequencies of protrusive cycles in invadopodia as well as frequencies of calcium spikes and MT1-MMP delivery to the invadopodia plasma membrane change in concert and are controlled by ECM cross-linking.

Switching between migration and invadopodia states is regulated by β1-integrin activity

The coordinated relationship between ECM properties and invadopodia dynamics and function suggest a central role for the outside-in signaling provided by ECM-integrin interactions. As mentioned above, β1-integrin is localized to invadopodia and in its absence, invadopodia maturation and ECM-degrading function are disabled (7). We hypothesized that interactions between ECM and β1-integrin are the master regulator of invadopodia dynamics and, consequently, of the length of time that cell will spend in the invadopodia state. We next tested this hypothesis in our model as well as experimentally.

In our model, the effect of cell-ECM interaction on invadopodia dynamics was examined by varying the adhesion constant (Ka) from 1 (Fig. 1 *E*) to 0.2 and 0.01 s^{-1} (Fig. 6 *A*). A decrease in Ka reflects lower cell-ECM adhesion strength. Whereas modifying ECM cross-linking alters adhesion strength externally by changing the number of ECM molecules proximal to the cell, adhesion strength can also be targeted by modifying the integrin ability to bind ECM. The model results suggest that a decrease in adhesion strength (Ka = 0.2) will cause a decrease in the period spent in the invadopodia state, simultaneously increasing the time spent in the migration state to the point where invadopodia are completely eliminated and the cell continuously migrates (Ka = 0.01).

To test the simulation results, β1-integrin's ability to bind to the ECM was increasingly blocked using different doses of a monoclonal blocking antibody (4B4). The extent of invadopodia degradation and the average lengths of both invadopodia and migration states, which occur on the timescale of hours, were measured at various doses of 4B4. Results show that with increasing concentrations

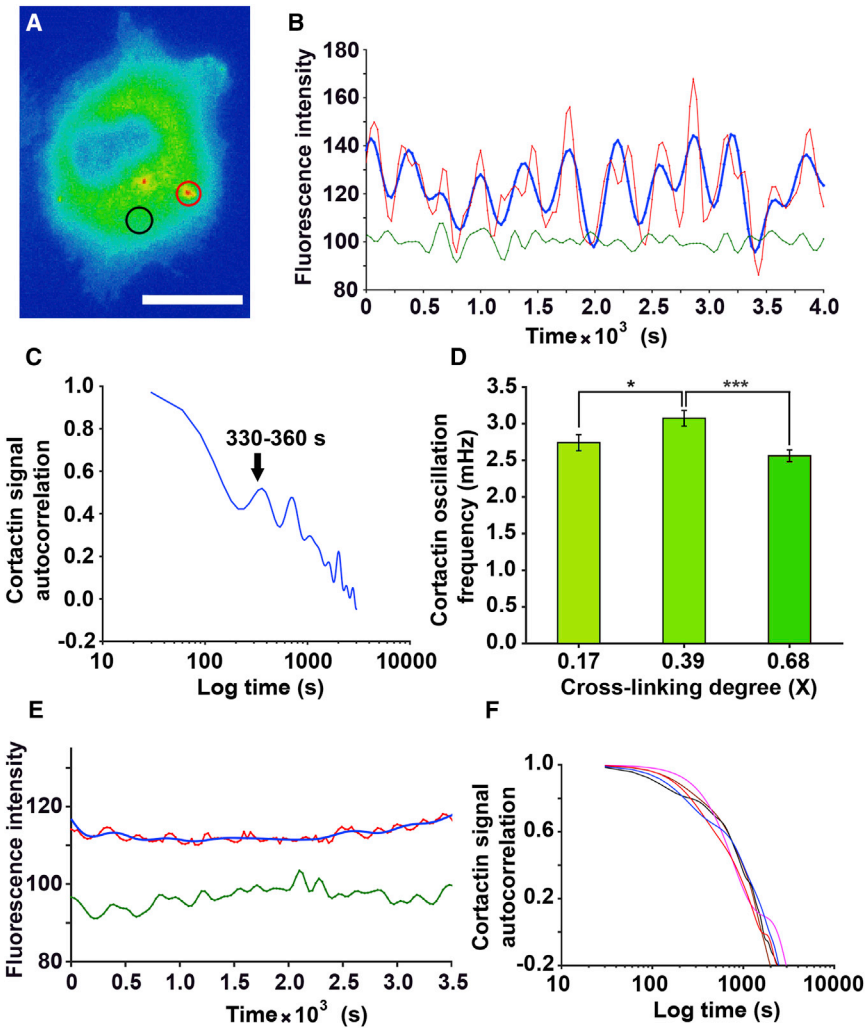

FIGURE 4 The frequency of cortactin oscillations is biphasically regulated by ECM cross-linking. (*A*) Shown is a representative pseudocolored image of a Cerulean-cortactin-MTLn3 cell. The invadopodium is circled in red, whereas the same size of area in the cytoplasm is circled in black. The signal inside the cytoplasmic circle is used as a filter for the cortactin signal in the invadopodium. (*B*) Shown are representative traces of cortactin signal oscillations (*red line*), cytoplasmic signal representing the noise (*green line*), and filtered cortactin signal (*blue line*) corresponding to areas within the circles in (*A*). (*C*) Shown is an autocorrelation analysis of the filtered cortactin signal showing the periodicity of the signal. (*D*) Bars show the cortactin oscillation frequency at different ECM cross-linking ratios and represent >10 cells per experiment and three separate experiments per condition. (*E*) Cortactin fluorescence over time is shown, measured in a cell treated with the F-actin inhibitor cytochalasin D (Movie S4). Fluorescence was measured in the invadopodia precursor (*red line*, before filtering; *blue line*, after filtering) and in the cytoplasm (*green line*). (*F*) Autocorrelation of cortactin signals in five cells with invadopodia precursors shows cortactin oscillations are absent when F-actin polymerization is inhibited. Pairwise comparisons were done with a 0.39 cross-linking ratio condition. Errors are shown as mean ± SE. $*p < 0.05$, $***p < 0.01$. To see this figure in color, go online.

of 4B4, the average time that a cell spends in the invadopodia state decreases, whereas that of the migration state increases (Fig. 6, *B* and *C*). At 2.0 μg/mL of 4B4, ECM degradation is totally halted, and cells migrate continuously. Higher concentrations of blocking antibody also block migration and cause cell detachment from the gelatin layer ($\geq$4.0 μg/mL). Furthermore, we tested the effect of partial β1-integrin inhibition on the dynamics of invadopodia-related activities, such as cortactin oscillations, which occur on the timescale of minutes. Results show a significant decrease in the frequency of cortactin oscillations from 3.08 mHz in control cells to 2.39 mHz in cells with partial β1-integrin inhibition (Fig. 6 *D*). Such a decrease is reminiscent of the effect of extreme ECM cross-linking values (Fig. 4 *D*). Collectively, these results indicate that interactions between the ECM and β1-integrin are involved in regulating invadopodia-related dynamics on the timescale of minutes and, in turn, the frequency of switching between invadopodia and migration states on the timescale of hours (Fig. 6 *E*).

DISCUSSION

Invadopodia assembly and function have been well studied as measures of cancer cell invasiveness, but the relationship between invadopodia and cell translocation and the dynamics of these events were never directly addressed. Here, to our knowledge, we demonstrate for the first time that cancer cells with invadopodia repeatedly oscillate between invadopodia and migration states. Importantly, we show that the degree of ECM cross-linking controls the balance between the two states via the level of β1-integrin activity. Moreover, ECM cross-linking controls invadopodia dynamics and function, which involve protrusion-retraction cycles and calcium-dependent MT1-MMP delivery to the plasma membrane.

The increase in ECM cross-linking has been previously demonstrated to increase the number of focal adhesions (29) and invadopodia (2,14,39). Further, the stiffness of the ECM has been reported to affect invadopodia numbers and activity (15). Finally, either an increase in ECM

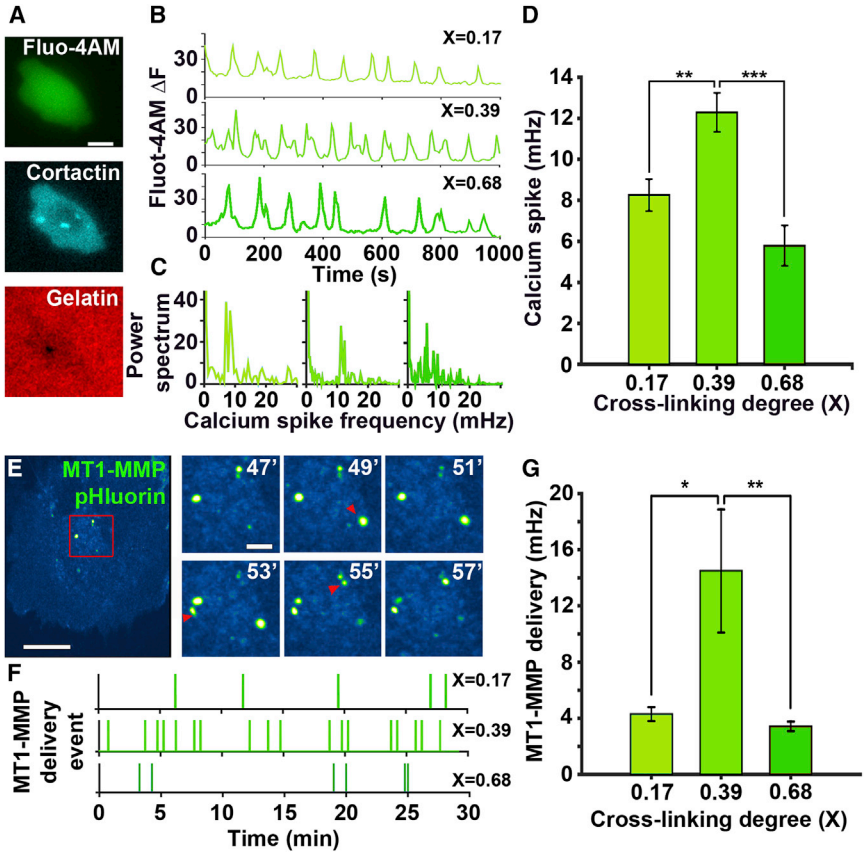

FIGURE 5 Frequencies of calcium spike and MT1-MMP vesicle delivery are biphasically regulated by ECM cross-linking. (*A*) Shown are representative fluorescence micrographs of Cerulean-cortactin-MTLn3 (*cyan*, *middle*) cells (see Movie S6) labeled with Fluo-4-AM (*green*, *top*), plated on fluorescent gelatin (*red*, *bottom*). Scale bars,10 microns. (*B*) Representative calcium spikes are shown, recorded in cells at different gelatin cross-linking ratios. (*C*) Shown is a power spectrum of calcium spikes in (*B*). (*D*) Shown is a comparison of average spike frequencies at different gelatin cross-linking ratios. Scale bars, 10 μm. Data include >15 cells per experiment for three separate experiments per condition. Pairwise comparisons were done with a 0.39 cross-linking ratio condition. (*E*) Shown is a representative image of an HS-578T cell transfected with MT1-MMPpHluorin (see Movie S6). The right panel depicts the dynamics of MT1-MMP containing vesicle delivery to the plasma membrane. The red arrows point at newly delivered vesicles. (*F*) Shown is the representative record of the MT1-MMP delivery event over 30 min in cells at different gelatin cross-linking ratios. (*G*) A comparison of the average frequency of MT1-MMP delivery is shown at different gelatin cross-linking ratios. Data include >15 cells per experiment for three separate experiments per condition. Pairwise comparisons were done with a 0.39 cross-linking ratio condition. Errors are shown as mean ± SE. $*p < 0.05$, $**p < 0.01$, $***p < 0.001$. To see this figure in color, go online.

stiffness or mechanical stretching of the ECM layer has been demonstrated to increase MMP expression (40,41). Here, we show that the increase in ECM cross-linking affects invadopodia-related dynamics and their ECM-degrading function. Although the number of precursors plateaus with the increase in cross-linking, the number of mature invadopodia demonstrates a pronounced biphasic trend, suggesting that the cross-linking variations may be more important in later steps of invadopodia assembly, such as maturation and MT1-MMP delivery steps. Our data on MT1-MMP recycling confirm this hypothesis. Collectively, our data demonstrate that intermediate levels of ECM cross-linking support the highest speeds of protrusive cycles as well as the most frequent MT1-MMP delivery via Ca^{2+} oscillations while making invadopodia more stable, resulting in a peak of degradative activity. Furthermore, the extent of interactions between ECM and β1-integrin dictates the length of time that a cell can spend in the invadopodia state and the frequency of switching between migration and invadopodia states.

Previous quantitative studies in both invadopodia—generated by cancer cells (13)—and podosomes—generated by macrophages or dendritic cells (11,42,43)—have shown an oscillatory behavior of the structure core, reflecting protrusion-retraction cycles. Intensity fluctuations in the core actin and cortactin content are a direct measure of the vertical movement of the protrusion tip "digging" into the ECM (11). Similar oscillations were seen in stiffness levels of the podosome structure itself, as measured by atomic force microscopy (42). Lengths of protrusion-retraction cycles (i.e., core oscillations) reported in various cell types were 300–900 s (11,13). Elimination of such cycles was seen with perturbations of actin core by inhibition of Rho-associated protein kinase or myosin light-chain kinase (11) or inhibition of cortactin phosphorylation (13). Our data suggest that the cell "sensing" of ECM cross-linking translates into frequency of protrusion-retraction cycles in a coordinated fashion. Thus, the ECM cross-linking degree optimal for maximal degradation is in coordination with the fastest protrusion-retraction cycles as well as the highest frequencies of calcium spikes and MT1-MMP delivery. Interestingly, coordination between calcium spikes and oscillations in cortical actin (as well as N-WASP and PI(4,5)P2) was recently demonstrated to be essential in vesicle secretion in leukemia cells (44,45).

In breast carcinoma (7) as well as metastatic melanoma (46), β1-integrin is localized to invadopodia. β1-integrin is also highly expressed in breast carcinoma compared to β3 and β5 and is necessary for invadopodia maturation, whereas β3's role focuses on general adhesions. Our model

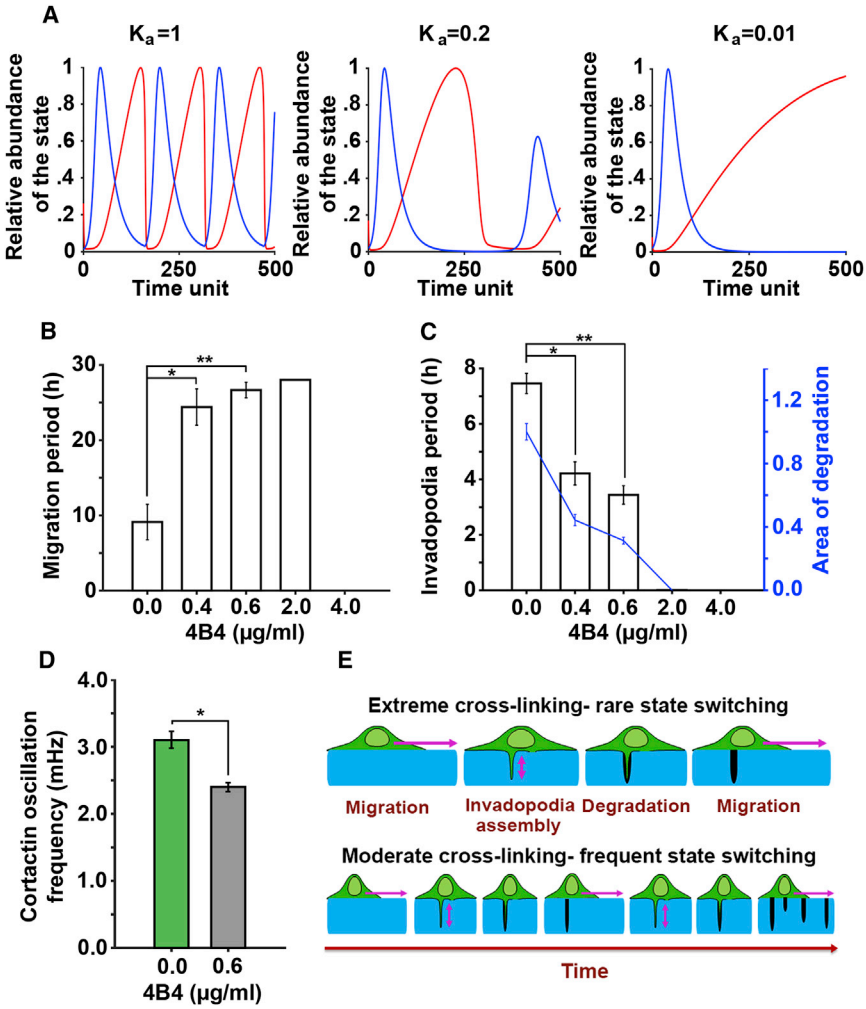

FIGURE 6 β1-integrin regulates balance between migration and invadopodia states. (*A*) Shown are the simulation results of the cancer cell oscillation between invadopodia (*blue*) and migration (*red*) for decreasing values of K_a, indicating the elimination of the invadopodia state at $K_a = 0.01$ (*right panel*). (*B*) The change in time spent in migration state (h) with increasing doses of β1-integrin blocker is shown. (*C*) The change in time spent in the invadopodia state (h) and invadopodia degradation with increasing doses of β1-integrin blocker 4B4 is shown. The blue line shows relative invadopodia degradation per cell (*blue axis*). Pairwise comparisons were done with the control condition (0 μg/mL 4B4). (*D*) Cortactin oscillation frequency is measured in cells treated with PBS (*green bar*) or cells treated with 0.6 μg/mL 4B4 β1-integrin inhibitor (*gray bar*). Experiments were done on a gelatin layer with a cross-linking degree of 0.39, in triplicate, and errors are shown as mean $\pm$ SE. $*p < 0.05$, $**p < 0.01$. (*E*) Shown is a summary of the conclusions. The levels of ECM cross-linking determine ECM-integrin interactions, which control the speed of invadopodia "digging" and ECM degradation. Faster invadopodia dynamics lead to more frequent switching between the invadopodia and migration states and, finally, to higher total ECM degradation. To see this figure in color, go online.

and results of blocking interactions between ECM and β1-integrin suggest that the balance between migration and invadopodia states can be altered via ECM-β1-integrin binding levels. Previous reports of dose response to soluble factors such as epidermal growth factor demonstrated similar biphasic trends of invadopodia numbers and/or chemotactic migration to increasing epidermal growth factor concentrations (47–49). Taken together, these data suggest that conditions in the extracellular environment cannot be directly taken as having a positive or negative effect on motility or invadopodia functions. Cells continuously adapt their behavior to match the conditions encountered in the extracellular environment, and this may include reverting to their invasive behaviors. It is possible that each stage of invadopodia assembly contains equilibrium points, and those invadopodia that do not reach stable conformation are continuously eliminated. Such a model is strengthened by a recent mathematical study on focal adhesion growth (50) suggesting that focal adhesions grow to the stable equilibrium length. Whereas the adhesions that did not reach equilibrium fully disassemble, those that surpass equilibrium size go through partial disassembly. Finally, stable focal adhesion size was found to be in direct relationship with ECM stiffness. In conclusion, our observations suggest the importance of considering nonlinear relationships between cells and their immediate environments, which are further complicated by receptor transactivation and inherent heterogeneities in cell transcription levels.

Data presented can be summarized in the model in which ECM-β1-integrin adhesion regulates the dynamics of invadopodia-related processes occurring on the timescale of minutes (speed of protrusion-retraction cycles and ECM degradation). This in turn regulates the dynamics of invadopodia-migration oscillations, which occur on the timescale of hours. Our data demonstrate that faster protrusion-retraction cycles are in conjunction with faster MT1-MMP recycling and calcium spikes, leading to faster ECM degradation. Next, this leads to invadopodia disassembly and cell translocation to a place with an intact ECM. In this model, integrin signaling regulates the speed and the efficiency of invadopodia short-scale dynamics, thus regulating long-scale dynamics of switches from the cell migration state

to the invadopodia state (Fig. 6 *E*). Our mathematical modeling strengthens this view. By simulating a wide range of conditions in a generalizable, nonparametric manner, the model predicts that changes in ECM-integrin binding and/or ECM cross-linking will induce changes in frequency of oscillations between migration and invadopodia states. Physically, this can be interpreted as a requirement for nonoverlapping levels of cell-ECM adherence in each of the states.

Our findings suggest the possibility of targeting invadopodia via ECM-modulation treatments. As invadopodia in vivo are necessary for intravasation (19) and extravasation (3)—and hence, metastasis (19)—an understanding of the relationships between the ECM and invadopodia carries powerful implications for future chemotherapies. If invadopodia and their degradative activity can be destabilized by minute changes in ECM cross-linking, this might potentially turn off the cancer cell metastatic potential. In vivo, there are several enzymes catalyzing covalent cross-links of collagen and elastin in cancer. These include lysyl oxidase, PLOD2, and TGII enzymes, all of which were linked to increased cancer cell motility and metastasis (51–53). Additionally, ECM cross-linking can be induced by nonenzymatic glycation between sugars and proteins, resulting in advanced glycation products that were shown to increase invasion in cancer cells (54). Reduction of ECM cross-linking via inhibitors specifically designed for lysyl oxidase, PLOD2, or TGII (48,55,56) as well as inhibitors of glycation such as flavonoids or aspirin (57) are likely to contribute toward invadopodia reduction. Our work suggests that such inhibitors can be valuable in reducing metastatic potential in neoadjuvant therapy.

SUPPORTING MATERIAL

Supporting Materials and Methods, two figures, one table, and six movies are available at http://www.biophysj.org/biophysj/supplemental/S0006-3495(18)30186-3.

AUTHOR CONTRIBUTIONS

A.B., K.E.P., and B.G. designed, analyzed, and interpreted all experiments and the mathematical model and wrote the manuscript. K.E.P. performed all experiments.

ACKNOWLEDGMENTS

We thank Dr. Ved Sharma and the lab of Dr. John Condeelis for the gift of the Cerulean-cortactin-MTLn3 cell line. We would like to also thank Dr. Philippe Chavrier for the gift of the MT1-MMPpHluorin plasmid. We thank Dr. Edna Cukierman, Dr. Evangelia Bellas, and Dr. Erica Golemis for help with editing this manuscript.

This work was funded by the National Institutes of Health grant 5K99CA172360, a Concern Foundation grant awarded to B.G., and National Institutes of Health grants R01CA164468 and R01 DA033788 awarded to A.B.

SUPPORTING CITATIONS

References (58–60) appear in the Supporting Material.

REFERENCES

1. Monsky, W. L., C. Y. Lin, …, W.-T. Chen. 1994. A potential marker protease of invasiveness, seprase, is localized on invadopodia of human malignant melanoma cells. *Cancer Res.* 54:5702–5710.
2. Gligorijevic, B., A. Bergman, and J. Condeelis. 2014. Multiparametric classification links tumor microenvironments with tumor cell phenotype. *PLoS Biol.* 12:e1001995.
3. Leong, H. S., A. E. Robertson, …, J. D. Lewis. 2014. Invadopodia are required for cancer cell extravasation and are a therapeutic target for metastasis. *Cell Reports.* 8:1558–1570.
4. Oser, M., H. Yamaguchi, …, J. Condeelis. 2009. Cortactin regulates cofilin and N-WASP activities to control the stages of invadopodium assembly and maturation. *J. Cell Biol.* 186:571–587.
5. Artym, V. V., Y. Zhang, …, S. C. Mueller. 2006. Dynamic interactions of cortactin and membrane type 1 matrix metalloproteinase at invadopodia: defining the stages of invadopodia formation and function. *Cancer Res.* 66:3034–3043.
6. Beaty, B. T., and J. Condeelis. 2014. Digging a little deeper: the stages of invadopodium formation and maturation. *Eur. J. Cell Biol.* 93:438–444.
7. Beaty, B. T., V. P. Sharma, …, J. Condeelis. 2013. β1 integrin regulates Arg to promote invadopodial maturation and matrix degradation. *Mol. Biol. Cell.* 24:1661–1675, S1–11.
8. Beaty, B. T., Y. Wang, …, J. Condeelis. 2014. Talin regulates moesin-NHE-1 recruitment to invadopodia and promotes mammary tumor metastasis. *J. Cell Biol.* 205:737–751.
9. Monteiro, P., C. Rossé, …, P. Chavrier. 2013. Endosomal WASH and exocyst complexes control exocytosis of MT1-MMP at invadopodia. *J. Cell Biol.* 203:1063–1079.
10. Sun, J., F. Lu, …, S. Yang. 2014. STIM1- and Orai1-mediated Ca(2+) oscillation orchestrates invadopodium formation and melanoma invasion. *J. Cell Biol.* 207:535–548.
11. van den Dries, K., M. B. M. Meddens, …, A. Cambi. 2013. Interplay between myosin IIA-mediated contractility and actin network integrity orchestrates podosome composition and oscillations. *Nat. Commun.* 4:1412.
12. Steffen, A., G. Le Dez, …, P. Chavrier. 2008. MT1-MMP-dependent invasion is regulated by TI-VAMP/VAMP7. *Curr. Biol.* 18:926–931.
13. Magalhaes, M. A. O., D. R. Larson, …, J. Condeelis. 2011. Cortactin phosphorylation regulates cell invasion through a pH-dependent pathway. *J. Cell Biol.* 195:903–920.
14. Enderling, H., N. R. Alexander, …, A. M. Weaver. 2008. Dependence of invadopodia function on collagen fiber spacing and cross-linking: computational modeling and experimental evidence. *Biophys. J.* 95:2203–2218.
15. Parekh, A., N. S. Ruppender, …, A. M. Weaver. 2011. Sensing and modulation of invadopodia across a wide range of rigidities. *Biophys. J.* 100:573–582.
16. Alexander, N. R., K. M. Branch, …, A. M. Weaver. 2008. Extracellular matrix rigidity promotes invadopodia activity. *Curr. Biol.* 18:1295–1299.
17. Yu, X., and L. M. Machesky. 2012. Cells assemble invadopodia-like structures and invade into matrigel in a matrix metalloprotease dependent manner in the circular invasion assay. *PLoS One.* 7:e30605.
18. Tolde, O., D. Rösel, …, J. Brábek. 2010. The structure of invadopodia in a complex 3D environment. *Eur. J. Cell Biol.* 89:674–680.
19. Gligorijevic, B., J. Wyckoff, …, J. Condeelis. 2012. N-WASP-mediated invadopodium formation is involved in intravasation and lung metastasis of mammary tumors. *J. Cell Sci.* 125:724–734.

20. Wolf, K., M. Te Lindert, …, P. Friedl. 2013. Physical limits of cell migration: control by ECM space and nuclear deformation and tuning by proteolysis and traction force. *J. Cell Biol.* 201:1069–1084.
21. Zaman, M. H., L. M. Trapani, …, P. Matsudaira. 2006. Migration of tumor cells in 3D matrices is governed by matrix stiffness along with cell-matrix adhesion and proteolysis. *Proc. Natl. Acad. Sci. USA.* 103:10889–10894.
22. Sharma, V. P., D. Entenberg, and J. Condeelis. 2013. High-resolution live-cell imaging and time-lapse microscopy of invadopodium dynamics and tracking analysis. *Methods Mol. Biol.* 1046:343–357.
23. Schindelin, J., I. Arganda-Carreras, …, A. Cardona. 2012. Fiji: an open-source platform for biological-image analysis. *Nat. Methods.* 9:676–682.
24. Orban, J. M., L. B. Wilson, …, D. A. Vorp. 2004. Crosslinking of collagen gels by transglutaminase. *J. Biomed. Mater. Res. A.* 68:756–762.
25. Grover, C. N., J. H. Gwynne, …, R. E. Cameron. 2012. Crosslinking and composition influence the surface properties, mechanical stiffness and cell reactivity of collagen-based films. *Acta Biomater.* 8:3080–3090.
26. Sage, D., F. R. Neumann, …, M. Unser. 2005. Automatic tracking of individual fluorescence particles: application to the study of chromosome dynamics. *IEEE Trans. Image Process.* 14:1372–1383.
27. Hamadi, A., G. Giannone, …, P. Rondé. 2014. Glutamate involvement in calcium-dependent migration of astrocytoma cells. *Cancer Cell Int.* 14:42.
28. Tinevez, J. Y., N. Perry, …, K. W. Eliceiri. 2017. TrackMate: an open and extensible platform for single-particle tracking. *Methods.* 115:80–90.
29. Levental, K. R., H. Yu, …, V. M. Weaver. 2009. Matrix crosslinking forces tumor progression by enhancing integrin signaling. *Cell.* 139:891–906.
30. Ehrbar, M., A. Sala, …, M. P. Lutolf. 2011. Elucidating the role of matrix stiffness in 3D cell migration and remodeling. *Biophys. J.* 100:284–293.
31. Hoshino, D., N. Koshikawa, …, K. Ichikawa. 2012. Establishment and validation of computational model for MT1-MMP dependent ECM degradation and intervention strategies. *PLoS Comput. Biol.* 8:e1002479.
32. Palecek, S. P., J. C. Loftus, …, A. F. Horwitz. 1997. Integrin-ligand binding properties govern cell migration speed through cell-substratum adhesiveness. *Nature.* 385:537–540.
33. Li, A., J. C. Dawson, …, L. M. Machesky. 2010. The actin-bundling protein fascin stabilizes actin in invadopodia and potentiates protrusive invasion. *Curr. Biol.* 20:339–345.
34. Lyford, G. L., P. R. Strege, …, L. Farrugia. 2002. alpha(1C) (Ca(V)1.2) L-type calcium channel mediates mechanosensitive calcium regulation. *Am. J. Physiol. Cell Physiol.* 283:C1001–C1008.
35. Farrugia, G., A. N. Holm, …, J. L. Rae. 1999. A mechanosensitive calcium channel in human intestinal smooth muscle cells. *Gastroenterology.* 117:900–905.
36. Calabrese, B., I. V. Tabarean, …, C. E. Morris. 2002. Mechanosensitivity of N-type calcium channel currents. *Biophys. J.* 83:2560–2574.
37. Godbout, C., L. Follonier Castella, …, B. Hinz. 2013. The mechanical environment modulates intracellular calcium oscillation activities of myofibroblasts. *PLoS One.* 8:e64560.
38. Lizárraga, F., R. Poincloux, …, P. Chavrier. 2009. Diaphanous-related formins are required for invadopodia formation and invasion of breast tumor cells. *Cancer Res.* 69:2792–2800.
39. Lauzier, A., M. Charbonneau, …, C. M. Dubois. 2012. Transglutaminase 2 cross-linking activity is linked to invadopodia formation and cartilage breakdown in arthritis. *Arthritis Res. Ther.* 14:R159.
40. Milkiewicz, M., F. Mohammadzadeh, …, T. L. Haas. 2007. Static strain stimulates expression of matrix metalloproteinase-2 and VEGF in microvascular endothelium via JNK- and ERK-dependent pathways. *J. Cell. Biochem.* 100:750–761.
41. Seo, K. W., S. J. Lee, …, C. D. Kim. 2013. Mechanical stretch increases MMP-2 production in vascular smooth muscle cells via activation of PDGFR-β/Akt signaling pathway. *PLoS One.* 8:e70437.
42. Labernadie, A., C. Thibault, …, G. M. Charrière. 2010. Dynamics of podosome stiffness revealed by atomic force microscopy. *Proc. Natl. Acad. Sci. USA.* 107:21016–21021.
43. Labernadie, A., A. Bouissou, …, I. Maridonneau-Parini. 2014. Protrusion force microscopy reveals oscillatory force generation and mechanosensing activity of human macrophage podosomes. *Nat. Commun.* 5:5343.
44. Smedler, E., and P. Uhlén. 2014. Frequency decoding of calcium oscillations. *Biochim. Biophys. Acta.* 1840:964–969.
45. Wollman, R., and T. Meyer. 2012. Coordinated oscillations in cortical actin and Ca2+ correlate with cycles of vesicle secretion. *Nat. Cell Biol.* 14:1261–1269.
46. Mueller, S. C., G. Ghersi, …, W. T. Chen. 1999. A novel protease-docking function of integrin at invadopodia. *J. Biol. Chem.* 274:24947–24952.
47. Philippar, U., E. T. Roussos, …, F. B. Gertler. 2008. A Mena invasion isoform potentiates EGF-induced carcinoma cell invasion and metastasis. *Dev. Cell.* 15:813–828.
48. Zhou, Z. N., V. P. Sharma, …, J. E. Segall. 2014. Autocrine HBEGF expression promotes breast cancer intravasation, metastasis and macrophage-independent invasion in vivo. *Oncogene.* 33:3784–3793.
49. Tönisen, F., L. Perrin, …, B. Gligorijevic. 2017. EP4 receptor promotes invadopodia and invasion in human breast cancer. *Eur. J. Cell Biol.* 96:218–226.
50. Cao, X., Y. Lin, …, V. B. Shenoy. 2015. A chemomechanical model of matrix and nuclear rigidity regulation of focal adhesion size. *Biophys. J.* 109:1807–1817.
51. Mangala, L. S., B. Arun, …, K. Mehta. 2005. Tissue transglutaminase-induced alterations in extracellular matrix inhibit tumor invasion. *Mol. Cancer.* 4:33.
52. Gilkes, D. M., S. Bajpai, …, G. L. Semenza. 2013. Procollagen lysyl hydroxylase 2 is essential for hypoxia-induced breast cancer metastasis. *Mol. Cancer Res.* 5:456–466.
53. El-Haibi, C. P., G. W. Bell, …, A. E. Karnoub. 2012. Critical role for lysyl oxidase in mesenchymal stem cell-driven breast cancer malignancy. *Proc. Natl. Acad. Sci. USA.* 109:17460–17465.
54. Sharaf, H., S. Matou-Nasri, …, N. Ahmed. 2015. Advanced glycation endproducts increase proliferation, migration and invasion of the breast cancer cell line MDA-MB-231. *Biochim. Biophys. Acta.* 1852:429–441.
55. Eisinger-Mathason, T. S. K., M. Zhang, …, M. C. Simon. 2013. Hypoxia-dependent modification of collagen networks promotes sarcoma metastasis. *Cancer Discov.* 3:1190–1205.
56. Jeitner, T. M., E. J. Delikatny, …, A. J. L. Cooper. 2005. Mechanism for the inhibition of transglutaminase 2 by cystamine. *Biochem. Pharmacol.* 69:961–970.
57. Peng, X., J. Ma, …, M. Wang. 2011. Naturally occurring inhibitors against the formation of advanced glycation end-products. *Food Funct.* 2:289–301.
58. Lauffenburger, D. A., and A. F. Horwitz. 1996. Cell migration: a physically integrated molecular process. *Cell.* 84:359–369.
59. DiMilla, P. A., K. Barbee, and D. A. Lauffenburger. 1991. Mathematical model for the effects of adhesion and mechanics on cell migration speed. *Biophys. J.* 60:15–37.
60. Ohuchi, E., K. Imai, …, Y. Okada. 1997. Membrane-type metalloproteinase digests extracellular matrix macromolecules including interstitial collagens. *Matrix Biol.* 16:76–77.

Biophysical Journal, Volume *114*

Supplemental Information

ECM Cross-Linking Regulates Invadopodia Dynamics

Kamyar Esmaeili Pourfarhangi, Aviv Bergman, and Bojana Gligorijevic

Model description

The mathematical model was developed based on the following assumptions and can be applied to any dimensionality of ECM architecture:

1. Average concentration of growth factor stimuli and intact, non-degraded ECM is assumed to be constant in the system;
2. High ECM concentration and crosslinking ratio can create physical barriers, inhibiting cell migration through the ECM (1, 2);
3. ECM degradation rate is assumed to exponentially decrease as ECM concentration is depleted (exponential decay);
4. The potential of the cell for ECM degradation is assumed to decay between two cycles of MMP delivery (3);
5. It is assumed that cells migrate in a constant speed in a condition when there is no physical barrier opposing the cell movement.

The sets of ordinary differential equations predicting the changes in these three variables are as follows:

$$\frac{dC_{ECM}}{dt} = K_a * M * C_{ECM}^2 \left({(C_{ECM}^* - C_{ECM})} \Big/ {(1+X)^n C_{ECM}^*} \right) - K_c\, I \left(1 - exp(-K_{ic} C_{ECM})\right) \quad \text{(Eq.1)}$$

$$\frac{dI}{dt} = K_{ci}\, I \left(1 - exp(-K_{ic} C_{ECM})\right) - K_i\, I \quad \text{(Eq. 2)}$$

$$\frac{dM}{dt} = K_m ({1}/{(1+X)^n}) V - K_{cm}\, M\, {C_{ECM}}/{C_{ECM}^*} \quad \text{(Eq. 3)}$$

The first term of Equation 1 captures the increase in the ECM concentration when a cell moves from an area where ECM was degraded to an area with high abundance of intact ECM. Hence, the extent of the migration (*M*) has a direct positive effect on the increase in the local ECM concentration. As the migration requires cell-ECM adhesions to be created in the cell front and dissociated at the cell rear (4), dependence of cell migration to cell-ECM adhesions will be nonlinear (5). To capture the non-linear role of adhesions, M is multiplied by $K_a C^2_{ECM}$. Next, increase in ECM concentration and cross-linking ratio will reduce the cell movement by reducing ECM pore size (1, 2). To introduce this hindering effect to Equation 1, the first term of this equation is multiplied by $\left({(C_{ECM}^* - C_{ECM})} \Big/ {(1+X)^n C_{ECM}^*} \right)$. Higher ECM concentration and cross-linking ratio decrease the value of this term, therefore decreasing the total value of the whole Equation 1 (dC_{ECM}/dt). In this term, exponent *n* is a constant dependent on cell and ECM geometry, adapting the equation for various types of ECMs and cells. The exponent *n* captures the non-linear effects of crosslinking in creating physical barriers against cell migration. The value of this exponent was determined experimentally (**Figure S1**). The second term of Equation 1 depicts the degradation rate of the intact ECM by proteolytic activity of invadopodia. It is assumed that ECM degradation would exponentially reduce with the level of intact ECM, due to lesser availability of non-degraded ECM for proteolysis.

The first term of Equation 2 is the rate at which a cell degrades ECM. The higher the levels of Invadopodia state (I) and ECM concentration (C_{ECM}), the higher is the rate of invadopodia degradation. In this model, it is assumed that between two protease delivery events, the potential of invadopodia proteolytic activity decreases due to lesser availability of protease molecules (eg.

MT1-MMP). The second term of Equation 2 captures this negative effect on the invadopodia degradation value.

Table S1. List of variables and constants used in the model

Variable/Constant	Description	Unit	Value	reference
C_I	ECM concentration	Dimensionless (Percentage)	100 to 0	NA
C^*_{ECM}	Intact ECM concentration	Dimensionless	100	NA
I	Invasion state abundance	Dimensionless	$I_0 = 1e10^{-6}$	NA
M	Migration state abundance	Dimensionless	$M_0 = 1$	NA
X	ECM crosslinking ratio	Dimensionless	0 to 1	NA
K_a	Cell-ECM adhesion constant	1/s	1	--
K_c	Unit adjusting constant	1/s	1	--
K_{ic}	MT1-MMP proteolysis rate constant	1/s	0.00201	(6)
K_{ci}	Unit adjusting constant	1/s	1	--
K_i	MT1-MMP turnover rate constant	1/s	1/26	(3)
K_m	Unit adjusting constant	1/μm	1	--
K_{cm}	Unit adjusting constant	1/s	1	--
V	Maximum migration speed	μm/s	0.083	(7)
n	Indicator of the ECM cross-linking ratio effect on cell migration	dimensionless	6 for 2D; 7 in 3D assay	This paper **Figure S1**

Equation 3 represents variations in the Migration state levels over time. We assume that each cell has a constant rate of migration in a condition when there is no physical barrier opposing the cell movement. In 2D environment, where there are no physical barriers present on the dorsal side of the cell, the increase in size and number of focal adhesions on the ventral side of the cell can mimic physical barrier. In the first term of Equation 3, this constant speed is denoted by *V*. However, the extent of ECM crosslinking affects this speed. An increase in ECM crosslinking ratio decreases ECM pore size, resulting in a decrease in the velocity of cell migration (2). We assumed that the cell speed non-linearly decreases as the crosslinking ratio increases. The second term of Equation 3 accounts for the physical barriers that ECM concentration is responsible for. As a cell degrades its surrounding ECM, C_{ECM} decreases which causes a decrease in C_{ECM}/C^*_{ECM}, resulting in a decrease in the ECM concentration role in opposing cell migration. The second term is then multiplied by the amount of the Migration state, because it is assumed that the higher the value of the Migration state, the higher are the effects of physical barriers on the cell migration.

The set of ordinary differential equations consisting of Equations 1-3 was simultaneously solved using the kinetic values as indicated in Table 1 and the following initial conditions

$CI_0 = C^*_{ECM} = 100$ (%, intact ECM at the beginning)

$M_0 = 1$

$I_0 = 1e10^{-6}$

M_0 and I_0 are initial values of migration and Invadopodia states. It is assumed that the cell is initially in Migration state, until it reaches a point where it switches to Invadopodia state.

Our model has no spatial terms defined and does not store information about ECM concentration distribution. The model assumes a fixed concentration of intact ECM prior to the arrival of cells with degradation capacity, and that cells always migrate to in the direction where intact ECM is present which in turn stimulates ECM degradation. Such locations can be either in areas not previously visited by the cell or in the vicinity of previously degraded punctae. As a result, new invadopodia assembles and matures and new ECM degradation punctae are formed. If a cell initiates invadopodia assembly at previously degraded punctae, disassembly will occur prior to invadopodia maturation due to the absence of adhesion ligands in the ECM (**Movie S1, S2**).

In regard to ECM role in Migration/Invadopodia oscillations, our model is adhesion-centric. As integrin molecules are well-known mechanosensors, physical forces are likely to influence adhesion strengths and numbers. However, we do not explicitly address physical force effect on the system. Surrogates of the physical force are introduced to the model in the Equation 3, where both increase in cross-linking and concentration of the ECM exert hindering effect towards the abundance of cell migration state (*M*) as well as the maximum migration speed (*V*). For example, the model assumes that when ECM cross-linking is negligible, all cells will "move" at a maximum velocity *V* and these values will both be lower at higher ECM cross-linking and/or concentration levels.

Supporting references:

1. Zaman, M.H., L.M. Trapani, A.L. Sieminski, D. MacKellar, H. Gong, R.D. Kamm, A. Wells, D.A. Lauffenburger, and P. Matsudaira. 2006. Migration of tumor cells in 3D matrices is governed by matrix stiffness along with cell-matrix adhesion and proteolysis. Proc. Natl. Acad. Sci. 103: 10889–10894.
2. Ehrbar, M., A. Sala, P. Lienemann, A. Ranga, K. Mosiewicz, A. Bittermann, S.C. Rizzi, F.E. Weber, and M.P. Lutolf. 2011. Elucidating the role of matrix stiffness in 3D cell migration and remodeling. Biophys. J. 100: 284–293.
3. Hoshino, D., N. Koshikawa, T. Suzuki, V. Quaranta, A.M. Weaver, M. Seiki, and K. Ichikawa. 2012. Establishment and validation of computational model for MT1-MMP dependent ECM degradation and intervention strategies. PLoS Comput. Biol. 8: 1–10.
4. Lauffenburger, D. a, and a L. Horwitz. 1996. Cell migration: A physically integrated process. Cell. 84: 359–369.
5. DiMilla, P.A., K. Barbee, and D.A. Lauffenburger. 1991. Mathematical model for the effects of adhesion and mechanics on cell migration speed. Biophys. J. 60: 15–37.
6. Ohuchi, E., K. Imai, Y. Fujii, H. Sato, M. Seiki, and Y. Okada. 1997. Membrane-Type metalloproteinase digests extracellular matrix macromolecules including interstitial collagens. Matrix Biol. 16: 76–77.
7. Gligorijevic, B., A. Bergman, and J. Condeelis. 2014. Multiparametric Classification Links Tumor Microenvironments with Tumor Cell Phenotype. PLoS Biol. 12.

Supplementary Figures:

Figure S1.

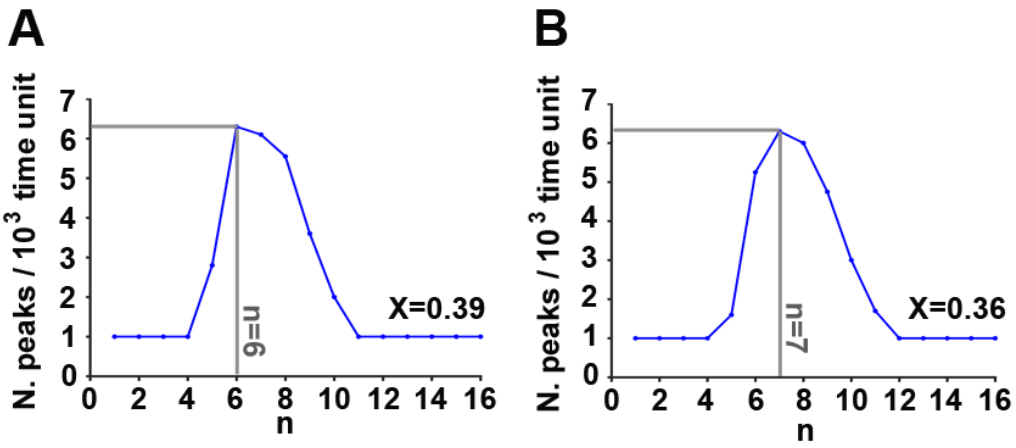

Figure S1. Fitting the value of n to the experimental data. In the model, cross-linking ratio was fixed to the optimal value measured experimentally (0.39 for 2D, 0.36 for 3D). The number of predicted invadopodia/migration switches over time was plotted at different values of n. The value of n with maximal number of switches was chosen, 6 for 2D (**A**) and 7 for the 3D (**B**) conditions.

Figure S2.

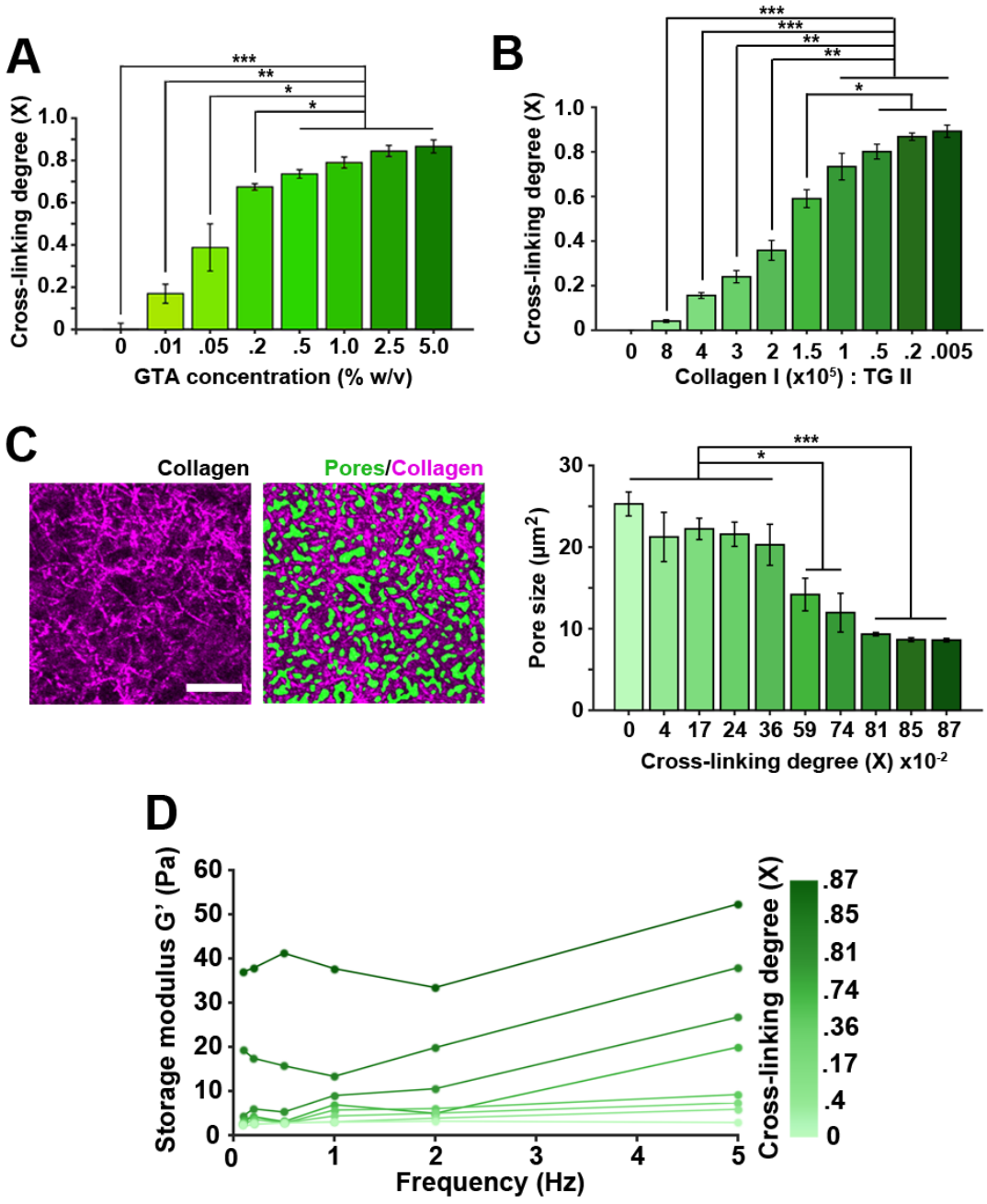

Figure S2. Measurements of physical properties of gelatin and collagen gels: A and B. Increase of the cross-linking ratio of the gelatin (A) and collagen gels (B) with increase in the cross-linker concentration. Errors are shown as SEM. **C.** Images of a representative 3D collagen gel taken by reflection confocal microscopy (raw image, left; processed image, right). Scale bar 5 µm. Bar graph shows pore sizes at different cross-linking degrees. T-test pairwise comparison performed among samples. P<0.05 *, P<0.01 **, P<0.001 *** **D.** Storage modulus of the collagen samples cross-linked with TG II, measured at 0.1-5 Hz frequencies of the strain control test.

Supplementary Movies

Supplementary Movie 1. MTLn3 cell switching from Migration to Invadopodia state.

Time lapse of Cerulean-cortactin-MTLn3 cells (left) cultured on Alexa 488-Gelatin (middle); overlay (right) used for measurements in Figure 1A-D. Centroid tracking is shown in blue and representative invadopodia are marked with red circles (starting 380 and 810 minutes). At the beginning of the movie, cell is migrating across the gelatin layer and assembles short-lived invadopodia precursors. When the cell centroid becomes stationary, the number of ECM-degrading invadopodia increases. Time between frames: 10 minutes. Scale bar is 10 μm.

Supplementary Movie 2. MDA-MB-231 cell switching between Migration and Invadopodia states. Time lapse movie acquired from a Cerulean-Lifeact-H2B-GFP-MDA-MB-231 cell (left) cultured on Alexa 488-gelatin (right). Centroid tracking is shown in blue and invadopodia are denoted by red circles (Starting at 110, 370 and 520 min). Time between frames: 10 minutes. Scale bar 10 μm.

Supplementary Movie 3. Oscillations of cortactin fluorescent signal in invadopodia

Representative example of time lapse recording of Cerulean-cortactin-MTLn3 cells (left) on gelatin with 0.39 cross-linking degree, used for cortactin oscillation measurements in **Figure 4B**. The cortactin punctae were filtered by Laplacian of Gaussian filter (right, Log 3d). Inserts zoom-in to an individual invadopodium. Time between frames: 30 seconds. Scale bars are 10 μm in the left and right panels and 5 μm in the inserts.

Supplementary Movie 4. Absence of cortactin oscillations upon F-actin polymerization inhibition by Cytochalasin D.

Representative example of time lapse recording of Cerulean-cortactin-MTLn3 cells (left) cultured on gelatin with 0.39 cross-linking degree and treated with 4 μM Cytochalasin D. Invadopodia precursors, visible as cortactin punctae, were filtered by Laplacian of Gaussian filter (right, Log 3d). Inserts zoom-in to an individual precursor. Time between frames: 30 seconds. Scale bars are 10 μm in the left and right panels and 5 μm in the inserts.

Supplementary Movie 5. Dynamics of calcium spikes measured by Fluo-4-AM.

Representative example of time lapse recording of Cerulean-cortactin-MTLn3 cells on gelatin with 0.39 cross-linking degree. Cells were loaded with Fluo4-AM and used to measure calcium spikes in **Figure 5A-D**. Time between frames: 5 seconds. Scale bar is 10 μm.

Supplementary Movie 6. Dynamics of MT1-MMP vesicle delivery to the plasma membrane.

Representative example of time lapse recording of HS-578T-MT1-MMP-pHluorin cells on gelatin with 0.39 cross-linking degree, used to measure frequency of delivery of MT1-MMP containing vesicles to the plasma membrane in **Figure 5E-G**. Cross-linking degree of 0.39 is shown. Time between frames: 30 seconds. Scale bar is 10 μm.